The structure of an essential splicing element: stem loop IIa from yeast U2 snRNA

Sarah C Stallings[1] and Peter B Moore[1,2]*

Background: Eukaryotic genes are usually transcribed as precursor mRNAs which are then spliced, removing introns to produce functional mRNAs. Splicing is performed by the spliceosome and provides an important level of post-translational control of gene expression. Stem loop IIa from U2 small nuclear (sn)RNA is required for the efficient association of the U2 small nuclear ribonuclear protein (snRNP) with the nascent spliceosome in yeast. Genetic analysis suggests that stem loop IIa is involved in RNA–protein interactions early in splicing, and it may also interact with other RNA sequences in U2. The sequence of loop IIa is well conserved, consistent with the idea that this loop is important for function.

Results: We have solved the structure of U2A, a 20-base analogue of stem loop IIa from *Saccharomyces cerevisiae*, using NMR and restrained molecular dynamics. In the process, we have demonstrated the efficacy of a new structure calculation protocol, torsion angle molecular dynamics. The structure that has emerged, which is consistent with the *in vivo* chemical protection data available for stem loop IIa in the context of intact U2 snRNA, contains a sheared GA pair followed by a U-turn in the loop. The U-turn conformation, which resembles the U-turns in tRNA anticodon loops, makes this stretch of U2 snRNA an obvious target for interactions with proteins and/or other RNA sequences.

Conclusions: The phenotypes of many stem loop IIa mutants can be rationalized assuming that the U-turn conformation in the loop must be preserved for efficient splicing. This observation, combined with the phylogenetic conservation of its sequence, suggests that the conformation of the loop of stem loop IIa is essential for its function in pre-mRNA splicing.

Addresses: [1]Department of Molecular Biophysics and Biochemistry, 266 Whitney Avenue, New Haven, CT 06520-8114 , USA and [2]Department of Chemistry, Yale University, PO Box 208107, New Haven, CT 06520-8107, USA.

*Corresponding author.
E-mail: moore@proton.chem.yale.edu

Key words: NMR, pre-mRNA splicing, RNA structure, torsion angle, U2 snRNA, U-turn

Received: **9 June 1997**
Revisions requested: **2 July 1997**
Revisions received: **23 July 1997**
Accepted: **31 July 1997**

Structure 15 September 1997, **5**:1173–1185
http://biomednet.com/elecref/0969212600501173

Introduction

In eukaryotic gene expression, nuclear pre-mRNAs are spliced prior to translation [1,2]. A ribonucleoprotein complex called the spliceosome assembles at splice sites and catalyzes the transesterification reactions required for intron excision and exon religation [3–5]. The hypothesis that pre-mRNA splicing is catalyzed by the RNA component of the spliceosome is strongly supported by the similarity between the mechanisms of spliceosome-catalyzed splicing and the self-catalyzed splicing of group II introns. In addition, there is a growing body of evidence indicating that RNA–RNA interactions both determine splice site choice and mediate formation of an active site in the spliceosome [6–9].

U2 small nuclear (sn)RNA is the RNA component of the U2 snRNP (small nuclear ribonucleoprotein), which is responsible for recognition of the intron sequence containing the 2′OH nucleophile, called the branchpoint, that attacks the 5′ splice site in the first transesterification reaction in splicing. In yeast, the addition of the U2 snRNP to the nascent spliceosome requires ATP, an appropriate branchpoint sequence in the pre-mRNA, and several protein factors [6,9–11]. Early in splicing, U2 snRNA base pairs with the branchpoint sequence [12,13]; later, it also pairs with U6 snRNA in interactions currently thought to contribute to the formation of the spliceosome's catalytic core [6–9,14,15].

Stem loop IIa, the focus of this investigation, is located just downstream of the branchpoint recognition sequence in U2 snRNA and comprises bases 48–67 in the *Saccharomyces cerevisiae* sequence. In this region of U2, methylation patterns following *in vivo* dimethyl sulphate (DMS) treatment are consistent with the secondary structure shown in Figure 1a, which includes a stem loop conformation for bases 48–67, but excludes base pairing between loop IIa (bases 54–61) and its phylogenetically conserved base-pairing complement downstream (bases 98–105). Compensatory mutation experiments have shown that base pairing within stem loop IIa is indispensable for splicing, but pairing between loop IIa and its downstream complement is not. Mutants lacking the entire downstream complement sequence are also viable [16]. The phylogenetic conservation of an apparently expendable base-pairing interaction

Figure 1

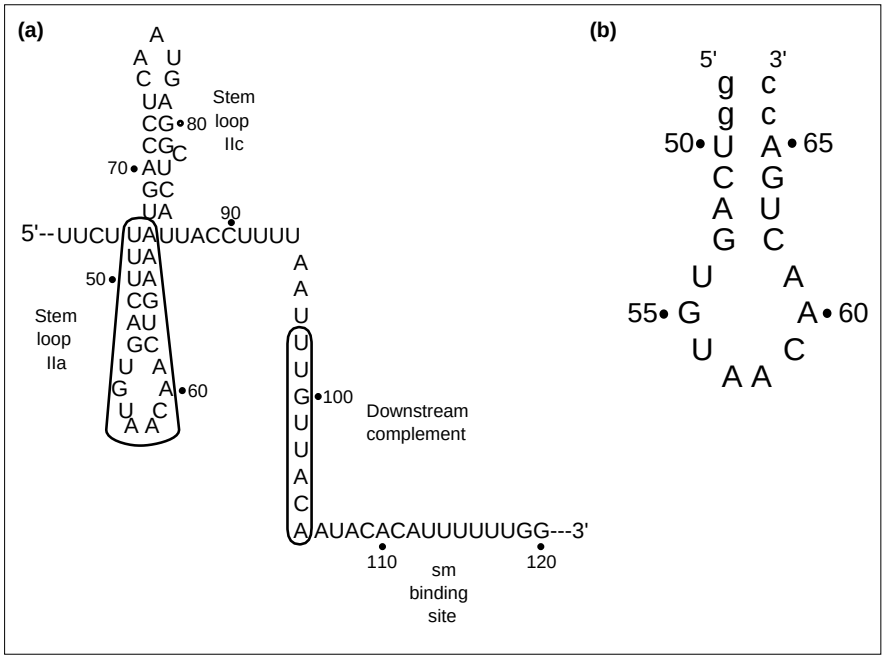

Stem loop IIa within intact U2 snRNA and the sequence of U2A. **(a)** The secondary structure of part of the 5′-end of yeast U2 snRNA, as determined by compensatory mutation analysis and *in vivo* DMS probing. Stem loop IIa and the loop IIa's downstream complement are circled. The binding site for the core set of conserved proteins common to all snRNPs involved in splicing, the sm proteins, is indicated. **(b)** The sequence of U2A, the molecule under study (see text). Lower case letters denote those residues in U2A which are changed from the *S. cerevisiae* sequence to facilitate T7 transcription.

between loop IIa and its downstream complement is difficult to understand [16,17].

Some single-base mutations in stem IIa result in a cold-sensitive phenotype characterized by a reduced rate of splicing *in vivo*, impaired U2 snRNP association with the assembling spliceosome *in vitro*, and a temperature-independent change in the secondary structure of U2 snRNA that results in the pairing of loop IIa with its downstream complement [18]. Interestingly, intragenic mutations in the downstream complement designed to disrupt pairing between it and loop IIa reverse both the temperature-dependent phenotype and the temperature-independent alternative secondary structure [17]. However, a second-site supressor mutation, which maps to a protein splicing factor required for the addition of U2 snRNP to the spliceosome, rescues the cold-sensitive phenotype, but does not restore the wild-type secondary structure of stem loop IIa [19]. In a synthetic lethality analysis of the cold-sensitive mutations, stem loop IIa was shown to interact with pre-mRNA processing proteins (PRPs) known to be required for the U2 snRNP assembly in the spliceosome [11]. Taken together, these results suggest that stem loop IIa is essential for splicing, that it forms part of the binding site for a multisubunit splicing factor required for the association of the U2 snRNP with the spliceosome in yeast and that the region of U2 snRNA containing stem loop IIa may adopt different conformations at different times during splicing [17–19].

The sequence of loop IIa is highly conserved, especially in positions 56–59, suggesting that these residues are functionally important. Nevertheless, some single base changes in invariant residues in loop IIa are viable mutations, as is a three-base change in residues 58–60 [16,20]. This certainly suggests that it is the structure of this loop that is important for its function, and not its sequence [16].

We have determined the solution structure of stem loop IIa by NMR using U2A, a 20-base RNA analogous to stem loop IIa from *S. cerevisiae*. We used a torsion angle molecular dynamics (TAMD) protocol to derive the structure of U2A from spectroscopic restraints [21,22]. By employing a reduced-variable description of the RNA conformation, this protocol samples conformational space much more efficiently than all-atom Cartesian search protocols. The convergence rate of structure calculations on U2A was significantly higher when using the TAMD protocol than when using a distance geometry/simulated annealing protocol.

The stem of stem loop IIa is a six base pair A-form stem, and its loop contains a sheared GA base pair followed by four bases in a U-turn conformation which resembles those seen in the anticodon loops of tRNAs. The conformation of the apex of the loop, which forces the Watson–Crick faces of the bases on the 3′-side of the loop to face into solution, may be important for the function of stem loop IIa in splicing.

Results and discussion

The U2A sequence was designed to have the same structure in isolation as that of stem loop IIa in intact U2 snRNA (Figure 1). The only difference between the two RNAs is that the two base pairs most distal from the loop,

Figure 2

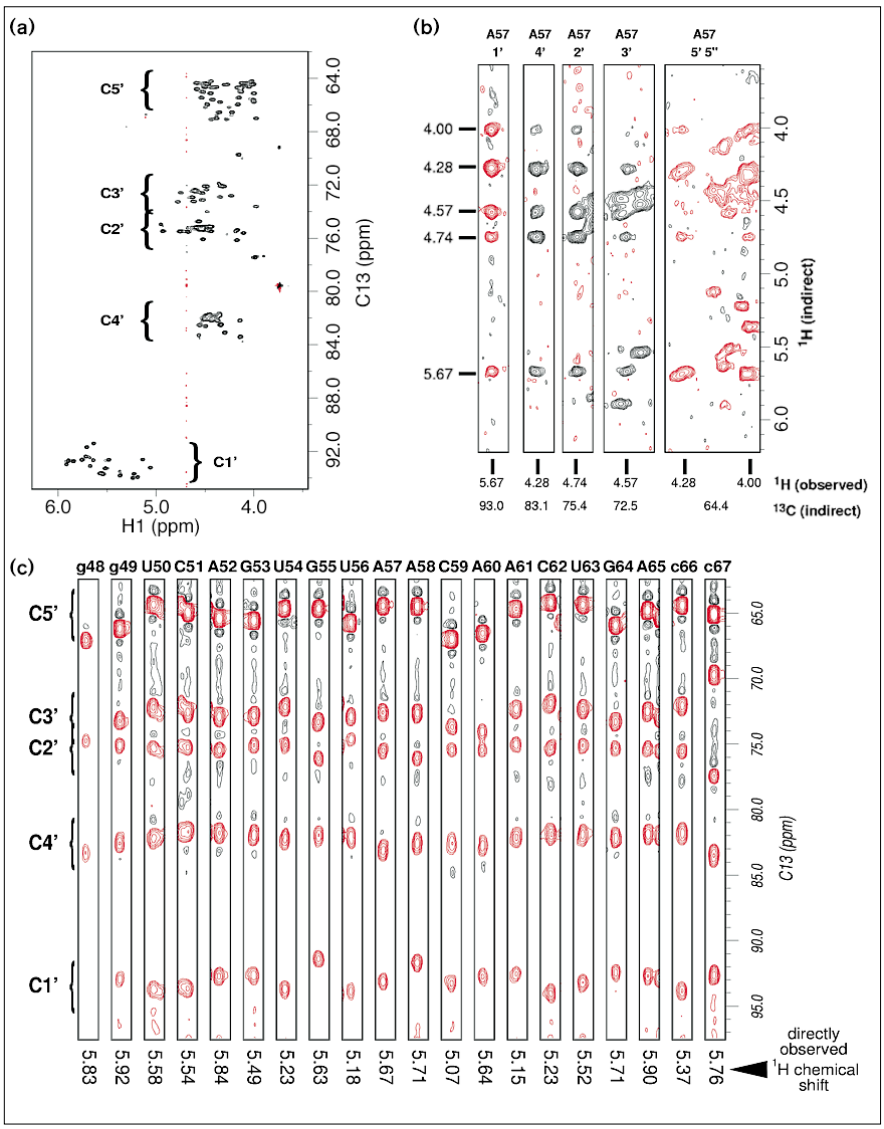

Assignment of ribose resonances in U2A. **(a)** The ribose region of a 2/J ^{1}H-^{13}C CT-HSQC experiment on U2A. **(b)** ^{1}H-^{1}H tiles from slices through the different ribose carbon regions of A57 from the 3D HcCH-TOCSY. Resonances in overlapped regions were assigned with the help of the carbon resolution in this experiment (e.g. H5′5″ in the spin system shown) or the redundancy of the information in the two data sets (e.g. H3′ in the spin system shown). **(c)** The twenty slices through the anomeric carbon chemical shift region of the 3D hCCH-TOCSY. Directly observed anomeric proton chemical shifts are given. The ribose carbon peaks in each tile are within the same ribose spin system, with the indirect carbon chemical shifts providing carbon assignments for each ribose associated to its anomeric resonance. These carbon chemical shifts were used to help identify the ribose protons in the HcCH-TOCSY. Red contours mark peaks with negative intensity, while black contours mark peaks with positive intensity.

which are UAs in stem loop IIa (U48–49 and A66–67), are changed to gcs in U2A (g48–49 and c66–67) to facilitate T7 transcription. (Upper case letters are used to designate bases found in both stem loop IIa and U2A; lower case letters denote bases in the sequence unique to U2A.) Mutations made in the two UA base pairs in question appear to have no effect on U2 snRNA function in yeast, as assayed by the viability of the mutant yeast [16].

Proton resonance assignment

As Figure 2a shows, the chemical shift dispersion in the ribose region of U2A's ^{1}H-^{13}C heteronuclear single quantum coherence (HSQC) spectrum is excellent, and this made it possible to identify the proton and carbon resonances for each ribose spin system using three-dimensional (3D) HcCH total correlation spectroscopy (TOCSY) and hCCH-TOCSY experiments done on a uniformly ^{13}C/^{15}N-labelled sample of U2A [23,24]. In these experiments, the same basic 3D TOCSY experiment was performed two ways: either by evolving the chemical shift of the proton resonance where the magnetization originates (HcCH-TOCSY) or by evolving the chemical shift of the carbon bonded to that proton (hCCH-TOCSY) (Figures 2b,c). Each anomeric resonance was correlated with the carbon resonances in its ribose using slices from the hCCH-TOCSY spectrum (Figure 2c), and once the carbon resonances were identified, the resonances of the ribose protons bonded to them could be assigned using HcCH-TOCSY data (Figure 2b). The only resonance not assigned in this way was the H3′ resonance of the 5′ terminus (g48), which was

Figure 3

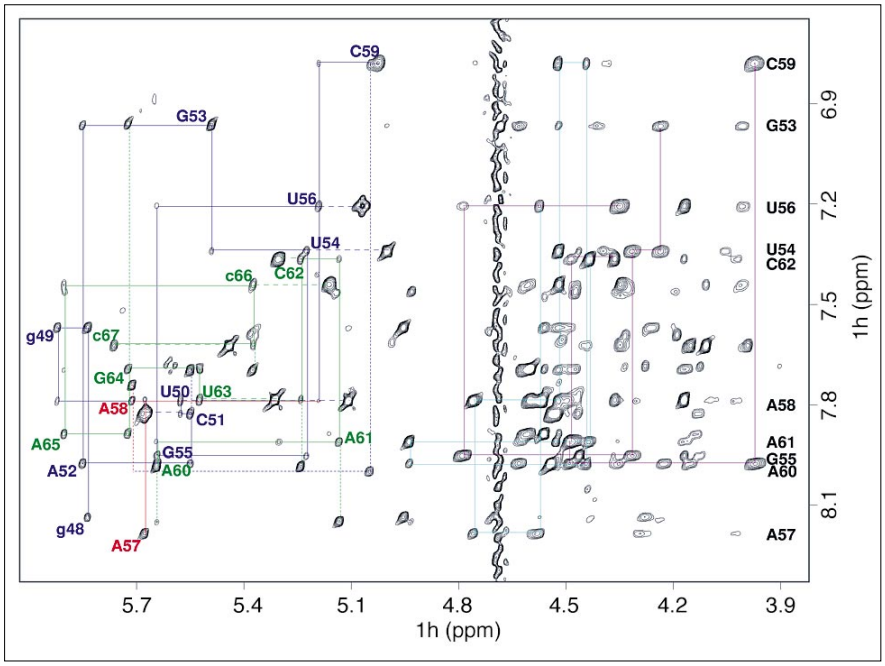

Sequential assignment of U2A. The ribose aromatic region of a 200 ms mixing time NOESY on U2A in D_2O showing the NOE correlations that were used to sequentially assign the molecule. The self aromatic–anomeric NOE cross-peaks are marked with the residue name and number. The anomeric–aromatic connectivities from g48 to C59 are shown in blue and those from c67 to A60 are in green. The connections between the adenines at the apex of the loop, which have few interresidue connections (see text) are shown in red. Dashed lines connect self anomeric–aromatic cross-peaks of pyrimidines to their self H5H6 cross-peaks, and dotted lines show adenine H2 to anomeric connectivities. Lines in cyan and magenta at the right of the spectrum trace aromatic to H2′ and aromatic to H3′ connectivities, respectively, through the residues in the loop, the aromatic chemical shift lines of which are indicated at the right-hand side of the spectrum.

assigned using nuclear Overhauser spectroscopy (NOESY) data. Assignments of the H2′ resonances were confirmed using a two-dimensional (2D) hCcH-COSY experiment, which correlated each H2′ proton to the anomeric carbon and proton resonances in the same ribose.

Non-exchangeable ^{1}H-^{1}H NOESY spectra were used to associate each sugar spin system with the aromatic protons of the base bonded to it, and to make sequential assignments (Figure 3). Adenine H2 resonances were correlated with their H8 resonances using a 2D HccH-TOCSY experiment, and pyrimidine self H5H6 cross-peaks were identified in a double quantum filtered correlation spectroscopy (DQF-COSY) experiment on unlabelled U2A. The anomeric–aromatic NOE correlations expected for an A-form helix are seen in the NOESY spectrum of U2A from its 5′-end to U56 and from A60 to its 3′-end. The most distinctive feature in its NOESY spectrum is a cross-strand NOE correlating U56H1′ with C59H6 (n to n+3) (Figure 3). It is accompanied by an intense NOE cross-peak between U56H1′ and C59H5 (not shown) and a weaker U56H1′ to A58H8 (n to n+2) correlation. H2′–aromatic and H3′–aromatic NOEs were used to assign A57 and A58 because their anomeric protons gave almost no interresidue NOEs.

The imino proton region of U2A's 2D NOESY in water contained few NOEs, and yielded no independent assignment information, even though a resolved resonance is observed for each G and U imino proton in 1D exchangeable proton spectra. The base type of each imino proton resonance was determined using a ^{15}N-^{1}H HMQC spectrum, and once the non-exchangeable proton resonances had been assigned, the imino proton resonances within Watson–Crick base pairs could be assigned from the few imino–X NOEs observable [25,26]. NOE cross-peaks between UH3 and AH2 protons identified the UA pairs in the stem (U50·A65 and A52·U63). The imino proton resonances of Gs in the stem GC pairs (g1·g20, g2·c19 and G53·C62) were assigned by correlating them with CH5 resonances. The two imino–imino NOE cross-peaks observed support these assignments.

At this point, only three upfield imino proton resonances remained unassigned: a GH1 resonance at 10.9 ppm (which, by elimination, had to be that of G55); and two UH3 resonances at 12.0 ppm and 11.2 ppm. Again by elimination, the two UH3 resonances must be U54H3 and U56H3, but it proved impossible to decide which was which. Neither imino proton has an NOE to A61H2, meaning that U54 and A61 are not paired, despite their juxtaposition in the sequence (Figure 1). Consistent with this conclusion, both of the imino proton resonances that could correspond to U54H3 have chemical shifts well upfield of the range expected for UH3s in Watson–Crick AU pairs. The DMS reactivity of A61 *in vivo* also suggests that it is unpaired [16].

The qualitative conclusion that can be drawn from these observations is that U2A is a stem loop, as expected, and that its secondary structure is fairly represented by the

Table 1

Proton assignments for U2A.

	H1/3	H6/8	H2/5	H1′	H2′	H3′	H4′	H5′	H5″
g48	13.28	8.14	na	5.83	4.95	4.71	4.55	4.43	4.27
g49	13.44	7.57	na	5.91	4.55	4.54	4.56	4.50	4.25
U50	14.40	7.79	5.10	5.56	4.52	4.33	4.36	4.58	4.12
C51	na	7.83	5.68	5.55	4.53	4.52	4.45	4.53	4.12
A52	na	7.98	6.96	5.85	4.64	4.61	4.48	4.54	4.15
G53	13.42	6.96	na	5.48	4.51	4.22	4.48	4.43	3.99
U54	nk	7.34	5.00	5.23	4.45	4.47	4.35	4.39	4.05
G55	nk	7.95	na	5.64	4.16	4.77	4.42	4.49	4.13
U56	nk	7.20	5.07	5.18	4.56	4.33	4.13	4.35	3.99
A57	na	8.20	7.76	5.68	4.75	4.58	4.28	4.23	4.01
A58	na	7.79	8.00	5.70	4.51	4.74	4.32	4.30	4.03
C59	na	6.78	5.03	5.05	4.43	3.96	4.49	4.36	3.96
A60	na	7.98	8.15	5.64	4.93	4.48	4.33	4.35	4.21
A61	na	7.91	7.99	5.13	4.43	4.48	4.42	4.44	4.16
C62	na	7.36	5.30	5.23	4.16	4.35	4.33	4.44	4.01
U63	13.48	7.78	5.32	5.52	4.58	4.30	4.39	4.49	4.08
G64	11.73	7.69	na	5.71	4.55	4.61	4.50	4.47	4.15
A65	na	7.88	7.70	5.89	4.49	4.58	4.43	4.59	4.13
c66	na	7.44	5.16	5.37	4.09	4.50	4.33	4.48	3.99
c67	na	7.62	5.44	5.76	3.98	4.49	4.14	4.44	4.00

The non-exchangeable proton resonances were assigned from spectra taken at 30°C and the exchangeable proton resonances from spectra taken at 15°C. Resonances not found in that residue's base type are referred to as 'na', and 'nk' refers to resonances whose assignment was not determined. H5′ and H5″ resonances were not stereospecifically assigned.

diagram in Figure 1b. The proton assignments for U2A are given in Table 1.

Dihedral angle restraints

The NMR spectra obtained for U2A contain considerable information about its dihedral angles. NOESY spectra of U2A contain no intense intraresidue aromatic–anomeric NOEs (see Figure 3), indicating that all its residues have glycosidic dihedral angles (χ) in the *anti* range [26]. Only two weak H1′H2′ cross-peaks were observed in the U2A DQF-COSY spectrum, and they belong to the 5′ and 3′ terminal residues. The ribose puckers of U2A residues 49–66, therefore, must be C3′-*endo*, and the ribose puckers of the two terminal residues, g48 and c67, are a mixture of conformations, and were not restrained in the structure calculation [27].

The dihedral angle ε was determined for all residues from C2′-P couplings measured using a spin-echo difference experiment [28,29]. $J_{C2'P}$ values less than 5 Hz are observed for ε in the *gauche*$^+$ or *trans* rotamers [30,31], and the *gauche*$^+$ rotamer is unavailable in RNA for steric reasons [32,33]. In U2A, only A57, A60, U56 and C59 gave measurable difference peaks in the experiment, but their C2′-P couplings were small, between 2 Hz and 3 Hz. For the remaining residues, $J_{C2'P}$ was less than 2 Hz. For all the residues of U2A, therefore, ε must be *trans* [30,31]. This agrees with other NMR data on U2A: the *gauche*$^-$ rotamer is possible only in ribonucleotides with C2′-*endo* sugar puckers, and, with the exception of the termini, there are none in U2A [27,30].

As spectroscopic evidence suggests A-form geometry in the base-paired stem, the dihedral angles α, β, γ and ζ, were restrained to A-form values for those residues. All residues in the loop are unrestrained about β. The dihedral angles α and ζ were broadly restrained about A-form values for those loop residues with A-form phosphorus chemical shifts [34]. Three phosphorus resonances in U2A have non-A-form chemical shifts. These resonances were assigned to U56-P-A57, A57-P-A58, and C59-P-A60 from their H3′ chemical shifts using a ^{31}P-^{1}H COSY spectrum. The α and ζ dihedral angles related to these phosphorus resonances were not restrained. The γ dihedral angles of residues U54 and A58 were restrained broadly to A-form values because both had two equally weak H5′ and H5″ to aromatic NOE cross-peaks, as expected when γ is *trans*. For the other six loop residues, resonance overlap made it impossible to observe these NOEs, and their γ dihedral angles were unrestrained.

The structure of U2A was determined using restraints for nearly all its dihedral angles (Table 2). Significantly, test calculations (discussed below) showed that restraints for sugar pucker, glycosidic dihedral angle, and ε and the distance restraints were sufficient to determine its structure.

Distance restraints

As the NOE cross-peaks observed for the stem of U2A were those predicted for A-form RNA, all proton–proton distances in the stem for which NOEs were observed were restrained to A-form values with 0.6 Å or 1 Å bounds. For

Table 2

Summary of restraints used in the structure calculation.

Restraint	Rationale	No.
Intraresidue proton distances		54
Interresidue proton distances	Observed NOE cross-peaks	83
AH2–other; non-sequential		5
Unoes	Unobserved NOE cross-peaks	12
χ	Self anomeric–aromatic NOE cross-peak intensity	20
Sugar pucker (ν_0–ν_4)	$J_{H1'-H2'}$	18
α and ζ	^{31}P chemical shift	30
Stem β	A-form NOE correlation patterns	12
Stem γ	A-form NOE correlation patterns	12
Loop γ	Aromatic–H5′H5″ NOE pattern	2
ε	$J_{C2'-P}$	19
Watson–Crick pair distances	Observed Watson–Crick	32
Planarity restraints on paired bases	Base pair NOE patterns	6

the loop residues, semi-quantitative distance restraints were derived from NOESY spectra collected in D_2O with 80, 140 and 200 ms mixing times. A total of 142 distance restraints were obtained this way (see Materials and methods section).

In addition, a small number of distance restraints were used to keep a few pairs of loop protons away from each other. The purpose of these restraints, which we call 'unoes', was to preclude conformations that imply NOEs that were not observed. Because NOEs can go undetected for many reasons, unoes were used sparingly, and all of them involved pairs of protons whose NOESY cross-peaks would have been clearly resolved if they had been present. Unoes were given ranges of 5 to 30 Å, 5 Å being a distance at the periphery of the observable NOE range and 30 Å being roughly the maximum distance in the molecule; 12 unoes were used. Calculations performed with and without the unoes proved that their use had no effect on the global structure of U2A, but that they did reduce the spread of the structure family (as discussed below).

Also included with the experimentally-derived restraints mentioned above were distance restraints defining the six base pairs in the stem, and planarity restraints to keep bases within base pairs coplanar. The restraints used in the structure calculation are summarized in Table 2.

Structure calculation

TAMD, a protocol that employs a reduced-variable search algorithm that permits only torsion angles to vary, was used to compute structures consistent with these restraints (Table 3) [21,22]. The starting template was a randomly extended nucleic acid chain with U2A's sequence and arbitrary dihedral angles. A set of structures was made using random initial velocities for each structure calculated. Accepted structures had restrained distances and dihedral angles that deviated from their set ranges by less than 0.2 Å and 2°, respectively, and bond lengths, bond angles and impropers that were within 0.02 Å, 2°, and 2°, respectively, of target values.

The TAMD protocol folded U2A efficiently, and did not require a distance geometry step to obtain acceptable convergence rates. Using TAMD, 80% of the molecular dynamics calculations resulted in accepted structures. The yield of accepted structures was much higher than that obtained using a distance geometry/simulated-annealing (DG/SA) protocol (80% versus 4%), while requiring only approximately three times the computational time using the same processor.

A randomly chosen set of 15 accepted TAMD structures was minimized using a protocol that employed attractive van der Waals and electrostatic potentials, and the average of the 15 structures was computed. The resulting family of

Table 3

Structure calculation protocol.

	High temperature TAMD	Cooling in torsion angle space	Cooling in Cartesian space	Conjugate gradient minimization	Gentle refinement
T (K)	20000	20000–300	3000–300	na	300
Step size (ps)	0.007	0.005	0.003	na	0.0005
Δtime (ps)	42	30	7.5	na	20
ω_{NOE}	2–50 (2–100)	100	150	200	50
ω_{cdih}	100	100	100	200	200
ω_{vdW}	5–0.3 (repel)	0.3–1 (repel)	1 (repel)	1 (repel)	1 (attractive)

Structure calculation protocol for U2A. Details of the torsion angle molecular dynamics (TAMD) and constant temperature molecular dynamics protocols used to calculate the structure of U2A are provided. Weights (ω) or temperatures (T) given as '*x* to *y*', were increased linearly from *x* to *y* during the time, Δtime. 'Repel' or 'attractive' in parentheses indicate the form of the van der Waals energy term used in the different stages of the structure calculation.

Figure 4

Conformational heterogeneity of the family of 15 minimized structures. All atoms of the 15 structures in the family were superimposed over **(a)** all residues, and **(b)** the loop residues of the average structure. The pair wise rmsds for the two superpositions (pair wise, each structure to the average) are 1.20 and 0.87 Å, respectively.

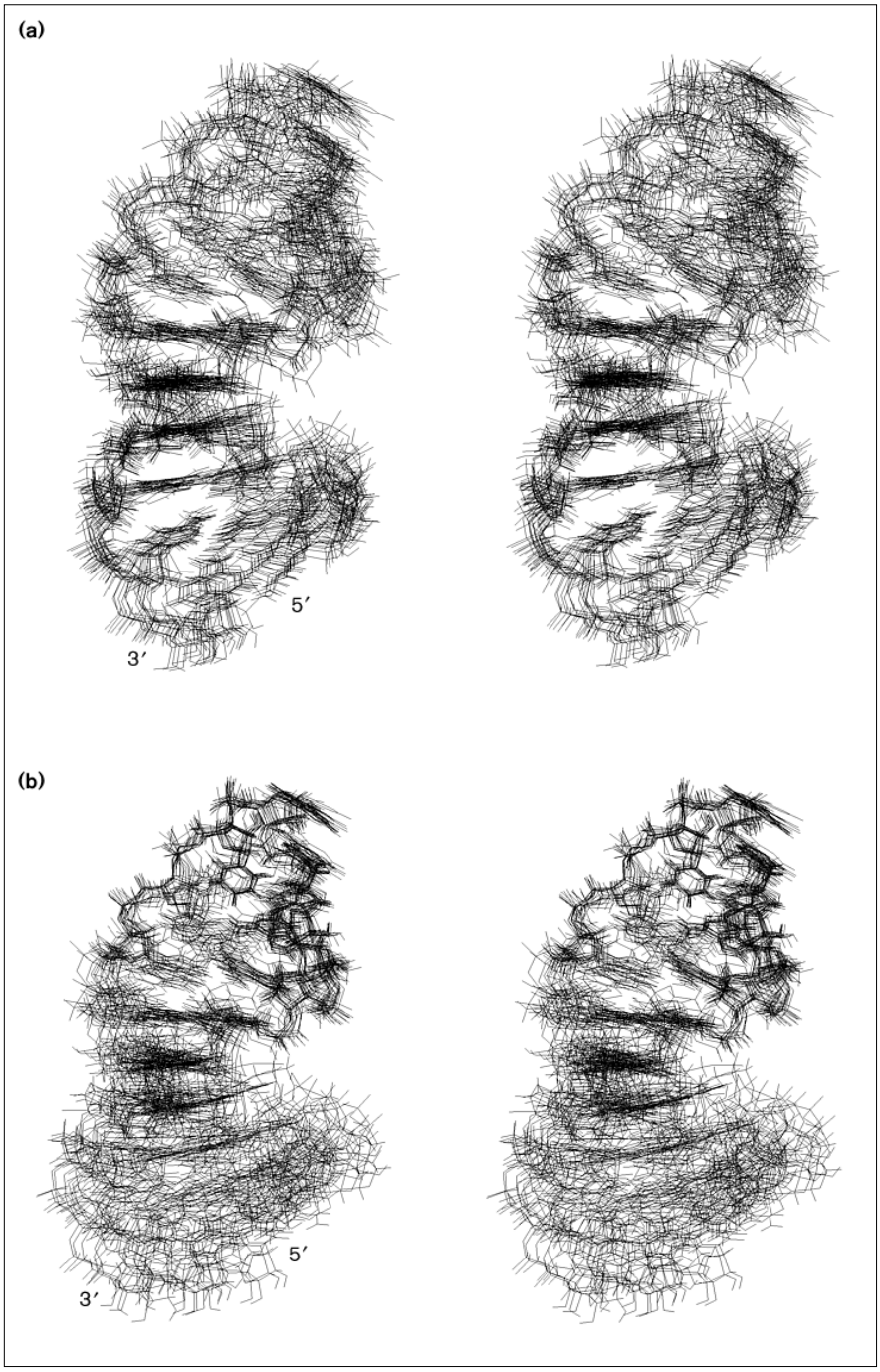

structures has no violations of distance restraints derived from NOEs greater than 0.2 Å, an average of one dihedral restraint violation greater than 2° (no 5° violations) and restraint root mean square deviations (rmsds) of 0.022 Å (NOE), 0.25° (dihedral), 0.0018 Å (bond length), 0.61° (angle) and 0.32° (improper). Figure 4a is an all-atom superposition of the 15 minimized structures on the average. The pair wise rmsd for all atoms of all residues of the family of 15 structure is 1.65 ± 0.53 Å (1.69 ± 0.56 Å for backbone atoms only); the all-atom pair wise rmsd for all structures to the average structure is 1.20 ± 0.36 Å (1.22 ± 0.37 Å for backbone atoms only). It is clear from the superposition of the loop atoms of the 16 structures (Figure 4b) that indeterminacy of the relative orientation of the loop with respect to the stem is a major source of the variation between structures. The mean pair wise rmsd of the 15 structures to their

Figure 5

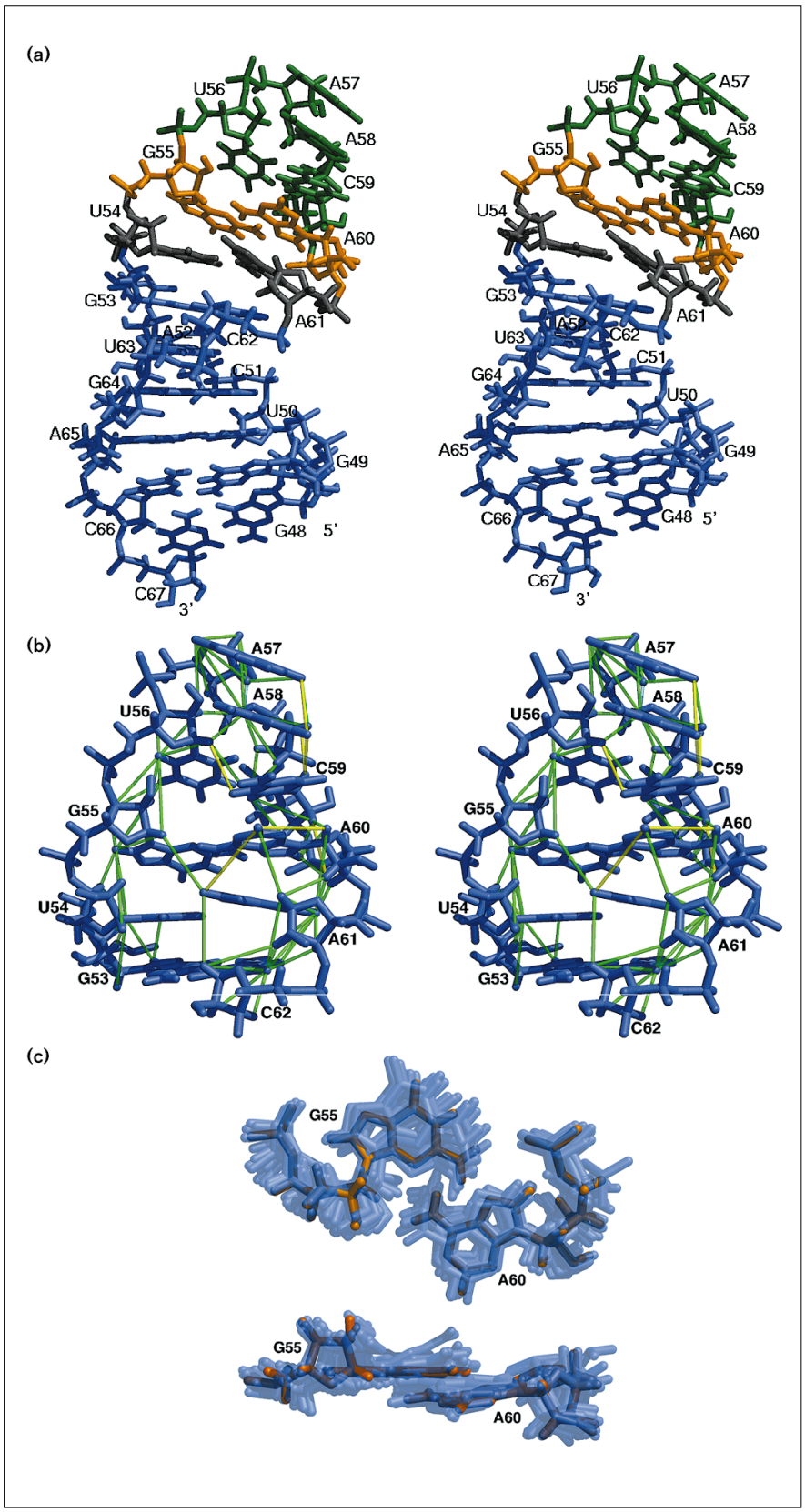

The structure of U2A. **(a)** A stereo view of the average of 15 minimized structures of U2A. Stem residues are in blue. In the loop, the sheared G55·A60 base pair is in orange and the U-turn (U56–C59) is in green. **(b)** A stereo view of the NOEs determining the conformation of loop IIa. Residues 52–62 are shown with the distance restraints from the structure calculation that correspond to intraresidue NOEs drawn between the protons. Green bars denote proton–proton distances that correspond to NOEs within their given range (d_{lower} to d_{upper}), and in yellow and cyan are the distances that are shorter and longer than their given ranges, respectively, but not outside of acceptance criteria (± 0.2 Å). **(c)** Two views of the sheared GA base pair formed between G55 and A60 in the loop. The average structure is in orange and the family of structures, superimposed on the average, is in blue.

average is 0.71 Å for all atoms of the loop residues only, and the corresponding rmsd for the stem residues is 0.86 Å. U56 is a loop residue remarkable for its relative lack of inter-residue NOEs, and the indeterminacy of its position is at least partly responsible for the observed indeterminacy of the relative orientation of the stem and the loop.

Validity of the refinement strategy

Some of the dihedral angle restraints used in the structure calculation are supported only indirectly by the NMR data: namely, the A-form restraints placed on the stem α, β, γ and ζ and loop α and ζ dihedral angles. In addition, the use of unoes is an unconventional method for precluding structures that imply NOEs that were not observed. The influence of both on the outcome of the structure calculations described was tested by repeating the TAMD protocol with different subsets of restraints. A set of 25 structures was calculated with only χ, sugar pucker and ε dihedral restraints, and another set of 25 structures was calculated with the unoe energy scaled to zero.

Neither reducing the number of dihedral restraints nor omitting unoes had an appreciable effect on the reproducibility or efficiency of the structure calculation: the acceptance rates were 72% (18/25) and 83% (20/24), respectively. In addition, the resultant average structures of the two test sets superimpose on all atoms of the average TAMD U2A structure with rmsds of 1.75 Å (reducing dihedral restraints) and 0.99 Å (omitting unoes) (0.79 Å and 0.76 Å, respectively, for all atoms of the loop residues). From these results, there is no reason to believe that any important features of U2A's structure were determined by the use of the additional dihedral angle or unoe restraints. What did change was the precision of the structure families. The rmsd with respect to the average of the structures computed with full restraints is significantly smaller than that of both sets of structures computed with the partial restraints, reflected in an increase in the conformational spread observed for the families of test structures.

The structure of stem loop IIa

The qualitative features of the structure of stem loop IIa are evident in Figure 5a. A six base pair stem is capped by a well-structured eight-base loop that contains a sheared GA base pair and a U-turn. U2A is stabilized primarily by stacking interactions. An eight-base stack, starting at g48 and extending to G55, stabilizes the 5′-side of stem loop IIa, and an 11-base stack from A57 to c67 stabilizes the 3′-side.

The most interesting part of the structure is the top of loop IIa where the backbone changes direction (U56–C59), which can be seen clearly in Figure 5b. This part of the structure superimposes on the U-turn at the apex of the anticodon loop of $tRNA^{Phe}$, whose sequence is UGAA [35], with an rmsd for backbone atoms (O5′, P, C5′, C4′, C3′ and O3′) of 1.37 Å. Clearly, loop IIa includes a U-turn.

The consensus sequence for the U-turn motif is UNRN, where N is any ribonucleotide and R is a purine. In U-turns, the backbone changes direction immediately following the initiating U, and the Watson–Crick faces of the bases immediately 3′ of the U are exposed to solvent. In the $tRNA^{Phe}$ crystal structure, this conformation is stabilized by a hydrogen bond between the imino proton of the first U and an oxygen of the phosphate of the third residue in the turn, and a hydrogen bond between the 2′OH of the U and the N7 of the n+2 purine (where n is the pivot of the turn). A van der Waals interaction between the pyrimidine ring of the U and the phosphate of the n+2 purine may also contribute to the stability [35]. The structure determined for stem loop IIa is consistent with these stabilizing interactions. In U2A, U56N3 is 3.60 Å from the phosphorus atom of C59's phosphate, and U56O2′ is 3.06 Å from A58N7; both of the hydrogen bonds seen in the $tRNA^{Phe}$ crystal structure could form in U2A. In addition, the phosphate of A58 sits directly over the pyrimidine ring of U56 (see Figure 5).

Although no restraints in the structure calculation paired G55 with A60, all low-energy models computed place G55 and A60 in a sheared (type II, *anti–anti*) GA pair below the U-turn (Figure 5c). The N7 of A60 is within hydrogen-bonding distance of the N2 protons of G55, and the N3 of G55 is within hydrogen-bonding distance of the N6 protons of A60. This pairing places the anomeric proton of A61 directly below A60's ring, and, consistent with this observation, A61's anomeric resonance is distinctly upfield shifted, as has been seen in other sheared GA pairs [36, 37]. G55's imino proton resonates at 10.9 ppm, well upfield of the chemical shifts seen for G imino protons in GC pairs, but in the range normal for G imino protons in this type of base pair [36,37]. G55's imino proton may be involved in a water-mediated hydrogen bond to the phosphate of A60 [38].

As pointed out earlier, the two remaining residues in the loop, U54 and A61, are not base paired, but it is not obvious why. All we can suggest is that the alignment of A61 with A60 maximizes stacking interactions that more than compensate for the hydrogen-bond energy lost. In contrast to three NOEs that fix the position of the base of A61, including an A61H2–A60H2 NOE, the data restrain the position of U54 much less tightly. The NOEs determining the structure of the loop are shown in Figure 5b.

Comparison with other RNA structures

The sequence of the hexanucleotide loop near the L11-binding site in 23S ribosomal RNA, GUAAUA, is nearly identical to that of the six nucleotides at the top of loop IIa, GUAACA. Not unexpectedly, the conformation of the hexanucleotide loop resembles that of loop IIa. Although the two structures recently reported for the hexanucleotide loop sequence differ in some respects, they agree that its

Figure 6

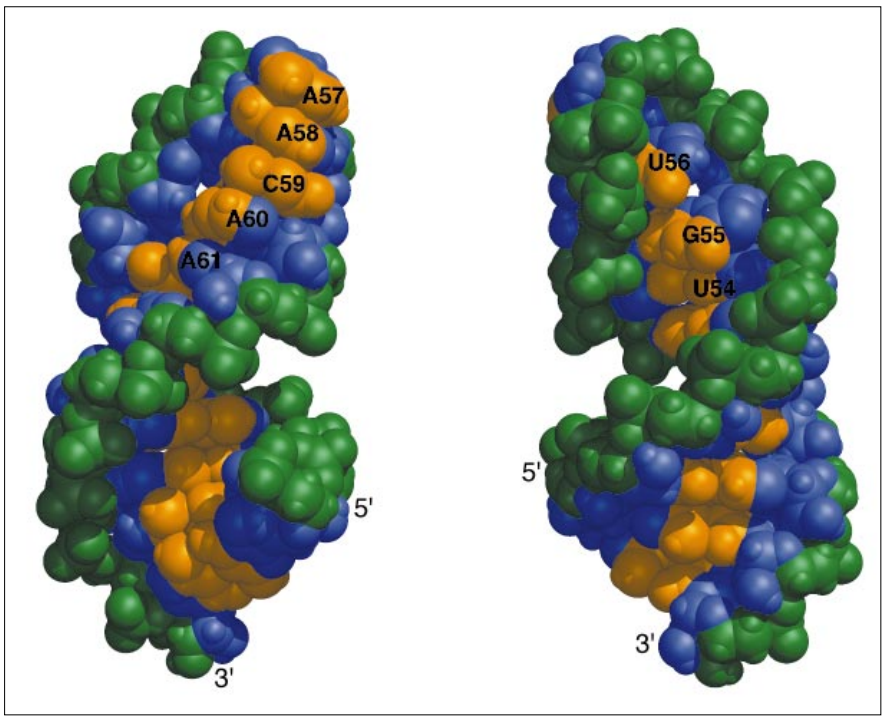

The structure of stem loop IIa has elements for protein or RNA recognition. Two space-filling models of stem loop IIa, related by 180° about the approximate helix axis. Watson–Crick faces are in orange, highlighting the faces of the residues 3′ of U56 that face into solution. The backbone atoms are in green, everything else is in blue.

conformation consists of a U-turn closed by a sheared GA pair, as seen in stem loop IIa [37,39]. This conformational similarity is reflected in the NMR data for U2A and one of the two hexanucleotide structures [37]. The NOESY spectra of both molecules include cross-strand NOEs between the anomeric proton of the U at the pivot of the turn (n) and the H5 and H6 protons of the pyrimidine at (n+3). The phosphorus resonances of the first two bases of the U-turn have downfield chemical shifts in both molecules, and the anomeric proton resonance of the base immediately 3′ to the A in the sheared GA pair has an upfield chemical shift, as does the imino proton resonance of its G. Thus the U-turn preceded by a sheared GA motif has a spectroscopic fingerprint that should make it easy to identify in other contexts in the future.

The U-turns in initiator and elongator tRNAs, which have the consensus U-turn sequence, have similar, but not identical, spectroscopic fingerprints [40]. As expected, a U anomeric to R aromatic NOE is observed, but no A-like U(n) anomeric to N(n+1) aromatic NOE. In addition, the phosphorus between the U(n) and N(n+1) nucleotides resonates downfield. Missing from the NMR data of anticodon loops are the U(n) anomeric to N(n+3) aromatic and H5 NOEs seen in the NMR spectra of U2A and the hexanucleotide loop [40]. This difference may reflect the fact that the U-turns in U2A and the hexanucleotide loop are closed by a sheared GA, but those in the anticodon loops are not.

The importance of the U-turn for stem loop IIa function

The consensus sequence for the apex of loop IIa is UAAY, and the U and the second A are universally conserved [16,20]. As mentioned before, some mutations in invariant residues in loop IIa are, paradoxically, viable in yeast, and now we can understand why. All of the mutations made in loop IIa that leave the UNRN U-turn sequence unaltered are viable, even those that change invariant residues [16]. It follows that the U-turn conformation of stem loop IIa must be important for its function. It may be important because it enables the two residues at the top of the loop (A57 and A58 in the wild-type sequence) to initiate the stacking interactions on the 3′-side of the structure. It may also be important because the Watson–Crick faces of the bases 3′ of the turn, which are exposed to solvent by its conformation (as seen in Figure 6) may be a site for stem loop IIa–protein or stem loop IIa–RNA interactions, as is the case in other systems [35,41–43].

The structure presented here also makes it possible to rationalize two viable loop mutants that do not conform to the UNRN pattern: CAAC and GAAC. The only stabilizing interaction seen in consensus UNRN U-turns that could not occur in a CAAC ‘U-turn’ is the imino proton-to-phosphate hydrogen bond discussed earlier. The GAAC sequence is nearly that of GNRA tetraloops, which have conformations similar to U-turns [44,45]. The GAAC sequence may, therefore, also support a turn having an acceptable geometry.

Some mutations in loop IIa are lethal. A five-base mutation of the loop IIa sequence that replaces the UAAC in positions 56–59 with UUUU is lethal, as is replacement of the entire loop with a UUCG tetraloop. A UUUU sequence is unlikely to adopt a conformation similar to the U-turn in wild-type loop IIa, and an octanucleotide loop to tetraloop change should be so perturbing to the loop geometry that it is hard to know what aspect of it is likely to be most damaging.

Biological implications

Pre-mRNA splicing is a specific processing event carried out by the evolutionarily conserved and highly specialized spliceosome. High-resolution structural studies of components in the spliceosome should contribute to the understanding of specific events in splicing, as they have for the ribosome and translation [46–48]. Only recently have unique functional domains of a size amenable to current structural techniques been identified in the spliceosome, and structural investigations have begun to be informative [49–52].

Stem loop IIa is essential for U2 snRNA function in yeast. It interacts with proteins known to be required for U2 snRNP association with the spliceosome, and it's disruption impedes that association. Stem loop IIa may also interact with a downstream sequence whose complementarity to the loop sequence is phylogenetically conserved.

The structure of loop IIa presented here has features that suit it for interaction with proteins and with RNA (Figure 6). Specifically, loop IIa contains a U-turn, an RNA structural motif that is known to engage in RNA–protein and RNA–RNA interactions in other systems. The bases immediately 3′ of the turn have their Watson–Crick faces exposed to solvent, ready to base pair with a complementary RNA strand, and present a distinctive hydrogen-bonding surface for protein recognition. The importance of the U-turn for function is supported by the results of mutagenesis studies, and by the conservation of the sequence of those residues in loop IIa. It appears that stem loop IIa uses the same conformational strategy as the anticodon loops of tRNAs to promote interactions with proteins and other RNAs.

Materials and methods

NMR samples

U2A was transcribed from a partially single-stranded DNA template using T7 RNA polymerase and either unlabelled (Pharmacia Biotechnologies) or fully ^{13}C- and ^{15}N-labelled nucleoside triphosphates [53]. Isotopically enriched nucleoside triphosphates were produced enzymatically from the nucleic acids of cells grown on enriched carbon and nitrogen sources [54–56]. The DNA oligonucleotides annealed to form the transcription template were chemically synthesized by the W M Keck Foundation Biotechnology Laboratory at Yale Medical School. The desired transcript was purified by gel electrophoresis and recovered using electroelution.

Purified U2A was dialyzed extensively against NMR buffer (10 mM KH_2PO_4, 50 mM KCl, 15 mM NaCl, 0.5 mM EDTA, pH 7.6) using 3000 MW cut-off dialysis tubing (Spectra-Por) and concentrated in a centricon-3 (Amicon) that had been treated with 0.1 M NaOH/2 mM EDTA, washed extensively with water and equilibrated in NMR buffer. D_2O to 10% v/v (to produce a lock signal) and dioxane to 1:500 v/v (used as an internal chemical shift standard) were added to the concentrated U2A sample. The U2A sample was transferred to a Shigemi microtube. NMR samples were approximately 180 µl of 1.5 to 3 mM U2A ($\varepsilon = 200.6$ mM/cm [OD]). For non-exchangeable proton NMR experiments, the sample was lyophilized in the Shigemi tube with the plunger removed and resuspended in 99.5% D_2O (Cambridge Isotopes) three times, then lyophilized and resuspended in 99.996% D_2O (Cambridge Isotopes).

NMR spectroscopy

Homonuclear proton and heteronuclear carbon/nitrogen/proton NMR spectra were collected either on a GE Omega 500 using a triple resonance probe with triple-axis gradients, or on a Varian Unity+ 600 spectrometer using a triple resonance probe equipped with a z axis gradient. Non-exchangeable proton spectra, homonuclear and heteronuclear, were collected at 30°C; exchangeable proton spectra were collected at 15°C. Spectra involving phosphorus were collected on the GE Omega500 using a triple resonance probe with a phosphorus coil and a z axis gradient. Collection parameters for the experiments discussed are given in a table which is available as supplementary material with the internet version of this paper.

Restraints in the structure calculation

The restraints used in the structure calculation are shown in Table 2. Distance restraints were determined semi-quantitatively from non-exchangeable NOESY spectra collected with a 7 s recycle delay between transients and 80, 140 and 200 ms mixing times. For the residues in the stem, judged to be A-form, proton–proton distances corresponding to observed NOEs were restrained to their A-form value, as given in Wüthrich [25], with ± 0.3 Å (for interresidue distances) or ± 0.5 Å (for intraresidue distances) ranges. For the residues at the junction of the stem and the loop (G53 and C62), all the ranges were ± 0.5 Å. For the residues in the loop, NOEs designated as 'strong' had intensities comparable to the H5-H6 cross-peak intensity in the 80 ms NOESY spectrum and were assigned a distance range of 1.9–3.4 Å. 'Medium' NOEs were present in the 80 ms NOESY spectrum with intensities less than those of H5–H6 cross-peaks and were assigned distance ranges of 2.0–4.5 Å. 'Weak' NOEs appeared in the 200 ms NOESY spectrum and could be seen weakly in the 140 ms NOESY spectrum; they were assigned distance ranges of 3.0–5.5 Å. For all residues, adenine H2 to anomeric proton distances were restrained to between 3 and 4.5 Å.

Unoes were included to keep the following pairs of protons apart from each other in the structure: G53H8:A52H8, G55H8:U56H6, U56H4′:A57H8, A57H8:A61H2, A58H8:C59H6, A58H2:C59H6, A58H2:A60H2, C59H6:A60H1′, A60H1′:C51H6, A60H1′:A61H1′, A60H1′:C59H1′, and A60H1′:C59H3′.

Backbone dihedral angles for the stem residues were restrained to A-form values [57]. Ribose sugar puckers for all but the terminal bases were determined to be C3′-*endo* on the basis of a lack of H1′-H2′ cross-peaks in the DQF-COSY, and were thus restrained using the N-type values for the five pseudo-rotation angles [27]. The glycosidic dihedral angles for all residues were restrained to 200° with 60° (stem) or 80° (loop) ranges. Dihedral restraints are shown in Table 2.

$J_{C2'\text{-}P}$ values were calculated from spin-echo difference spectra as described in Vuister *et al.* [28]. For the four residues with measurable, though weak (< 3 Hz), couplings, the dihedral angle ε was restrained to 200° ± 50°, and for the remaining residues with $J_{C2'\text{-}P}$ values within the noise, it was 200° ± 40°. Additional distance and dihedral restraints not derived directly from NMR data maintained the six base pairs in the stem.

Structure calculation

A structure file and starting coordinates for U2A were generated from the sequence of U2A using protocols derived from the generate.inp and generate_template.inp tutorial files in XPLOR [58]. The parameter and topology sets used were dna-rna-all atom.top and dna-rna-all atom.par available at ftp://proton.chem.yale.edu/pub/rna-structure. The dna-rna-all atom.par parameter set does not maintain the chirality of the nonbonded oxygens at the phosphates in the molecule. The resultant racemization has no effect on the structure calculation, but does artificially inflate the all-atom rmsds of the structures. We corrected the chirality after the structures were completed and before comparing the structures.

The TAMD refinement protocol used is presented in Table 3. The steps in the protocol were repeated using random initial velocities to build a family of structures. The major difference between this protocol and that described in Stein *et al.* is the slow introduction of NOE weights in the high-temperature step [22].

Acceptable TAMD structures were minimized employing switched van der Waals (includes attractive forces) and electrostatic potentials and a 1/R dielectric function.

Graphics

Molecular graphics images were produced using MidasPlus from the Computer Graphics Laboratory at UCSF (NIH RR-01081) and annotated either in Showcase (Silicon Graphics, Inc.) or CLRpaint (Stephen Bohus, University of Toronto).

Accession numbers

The coordinates of the 15 lowest energy structures and the distance and dihedral restraints used have been deposited at Brookhaven Protein Data Bank: accession numbers 1u2a (average structure coordinates) and 2u2a (coordinates of all 15 members of the structure ensemble).

Supplementary material

Supplementary material contains a table listing the collection parameters for the experiments discussed.

Acknowledgements

We thank Manual Ares, Jr for the advice and encouragement he has provided on numerous occasions, and Kevin MacKenzie and Luke Rice for technical assistance. This work was supported by a grant from the NIH (GM-41651).

References

1. Green, M.R. (1991). Biochemical mechanisms of constitutive and regulated pre-mRNA splicing. *Annu. Rev. Cell Biol.* **7**, 559–599.
2. Moore, M.J., Query, C.C. & Sharp, P. (1993). Splicing of precursors to mRNAs by the spliceosome. In *The RNA World.* (Gesteland, R.F. & Atkins, J.F., eds), pp. 303–357, CSHLab Press, Plainview, NY.
3. Guthrie, C. & Patterson, B. (1988). Spliceosomal snRNAs. *Annu. Rev. Genet.* **22**, 387–419.
4. Ruby, S.W. & Abelson, J. (1991). Pre-mRNA splicing in yeast. *Trends Genet.* **7**, 79–85.
5. Lamond, A.I. (1993). The Spliceosome. *Bioessays* **15**, 595–603.
6. Madhani, H.D. & Guthrie, C. (1994). Dynamic RNA–RNA interactions in the splicesome. *Annu. Rev. Genet.* **28**, 1–26.
7. Newman, A. (1994). Activity in the spliceosome. *Curr. Biol.* **4**, 462–464.
8. Sun, J.S. & Manley, J.L. (1995). A novel U2-U6 snRNA structure is necessary for mammalian mRNA splicing. *Genes Dev.* **9**, 843–854.
9. Ares, M., Jr. & Weiser, B. (1995). Rearrangement of snRNA structure during assembly and function of the spliceosome. *Prog. Nucl. Acid Res. Mol. Biol.* **50**, 131–159.
10. Ruby, S.W., Chang, T.-H. & Abelson, J. (1993). Four yeast spliceosomal proteins (PRP5, PRP9, PRP11, PRP21) interact to promote U2 snRNP binding to pre-mRNA. *Genes Dev.* **7**, 1909–1925.
11. Wells, S.E. & Ares, M., Jr. (1994). Interactions between highly conserved U2 small nuclear RNA structures and Prp5p, Prp9p, Prp11p, and Prp21p proteins are required to ensure integrity of the U2 small nuclear ribonucleoprotein in *Saccharomyces cerevisiae*. *Mol. Cell Biol.* **14**, 6337–6349.
12. Parker, R., Siliciano, P.G. & Guthrie, C. (1987). Recognition of the TACTAAC box during mRNA splicing in yeast involves base pairing to the U2-like snRNA. *Cell* **49**, 229–239.
13. Query, C.C., Moore, M.J. & Sharp, P. (1994). Branch nucleophile selection in pre-mRNA splicing: evidence for the bulged duplex model. *Genes Dev.* **8**, 587–597.
14. Madhani, H.D. & Guthrie, C. (1992). A novel base-pairing interaction between U2 and U6 snRNAs suggests a mechanism for the catalytic activation of the spliceosome. *Cell* **71**, 803–817.
15. McPheeters, D.S. & Abelson, J. (1992). Mutational analysis of the yeast U2 snRNA suggests a structural similarity to the catalytic core of Group I introns. *Cell* **71**, 819–831.
16. Ares, M., Jr. & Igel, A.H. (1990). Lethal and temperature-sensitive mutations and their supressors identify an essential structural element in U2 small nuclear RNA. *Genes Dev.* **4**, 2132–2145.
17. Zavanelli, M.I., Britton, J.S., Igel, A.H. & Ares, M., Jr. (1994). Mutations in an essential U2 small nuclear RNA structure cause cold-sensitive U2 small nuclear ribonucleoprotein function by favoring competing alternative U2 RNA structures. *Mol. Cell Biol.* **14**, 1689–1697.
18. Zavanelli, M.I. & Ares, M., Jr. (1991). Efficient association of U2 snRNPs with pre-mRNA requires an essential U2 RNA structural element. *Genes Dev.* **5**, 2521–2533.
19. Wells, S.E., Neville, M., Haynes, M., Wang, J., Igel, H. & Ares, M., Jr. (1996). CUS1, a supressor of cold-sensitive U2 snRNA mutations, is a novel yeast splicing factor homologous to human SAP-145. *Genes Dev.* **10**, 220–232.
20. Ares, M., Jr. & Igel, A.H. (1989). Phylogenetic comparison of U2 small nuclear RNA sequences suggests a pseudoknotted structure. *UCLA Symp. Mol. Cell. Biol.* **94**, 13–23.
21. Rice, L.M. & Brünger, A.T. (1994). Torsion angle dynamics: reduced variable conformational sampling enhances crystallographic structure refinement. *Proteins* **19**, 277–290.
22. Stein, E.G., Rice, L.M. & Brünger, A.T. (1997). Torsion angle molecular dynamics: a new, efficient tool for NMR structure calculation. *J. Magn. Reson. B* **127**, 154–164.
23. Clore, G.M., Bax, A., Driscoll, P.C., Wingfield, P.T. & Gronenborn, A.M. (1990). Assignment of the sidechain ^{1}H and ^{13}C resonances of interleukin-1β using double- and triple-resonance heteronuclear three-dimensional NMR spectroscopy. *Biochemistry* **29**, 8172–8184.
24. Nikonowicz, E.P. & Pardi, A. (1992). Simple procedure for resonance assignment of the sugar protons in ^{13}C-labeled RNAs. *J. Am. Chem. Soc.* **114**, 9202–9203.
25. Wüthrich, K. (1986). *NMR of Proteins and Nucleic Acids.* John Wiley & Sons, NY.
26. Varani, G. & Tinoco, I, Jr. (1991). RNA structure and NMR spectroscopy. *Q. Rev. Biophys.* **24**, 479–532.
27. Altona, C. (1982). Conformational analysis of nucleic acids. Determination of backbone geometry of single-helical RNA and DNA in aqueous solution. *Recueil Review: Journal of the Royal Netherlands Chemical Society* **101**, 413–433.
28. Vuister, G.W., Wang, A.C. & Bax, A. (1993). Measurement of three-bond nitrogen-carbon J couplings in proteins uniformly enriched in ^{15}N and ^{13}C. *J. Am. Chem. Soc.* **115**, 5334–5335.
29. Legault, P., Jucker, F.M. & Pardi, A. (1995). Improved measurement of ^{13}C, ^{31}P J coupling constants in isotopically labelled RNA. *FEBS Lett.* **362**, 156–160.
30. Mooren, M.W.W., Wijmenga, S.S., Marel, G.A. v.d., Boom, J.H. v. & Hilbers, C.W. (1994). The solution structure of the circular trinucleotide cr(GpGpGp) determined by NMR and molecular mechanics. *Nucl. Acids Res.* **22**, 2658–2666.
31. Varani, G., Aboul-ela, F. & Allain, F.H.-T. (1996). NMR investigations of RNA structure. *Prog. Nucl. Magn. Reson. Spectr.* **29**, 51–127.
32. Lankhorst, P.P., Haasnoot, C.A.G., Erkelens, C. & Altona, C. (1984). Carbon-13 NMR in conformational analysis of nucleic acid fragments 2. A reparameterization of the Karplus equation for vicinal NMR coupling constants in CCOP and HCOP fragments. *J. Biomol. Struct. Dyn.* **1**, 1387–1405.
33. Blommers, M.J.J., Nanz, D. & Zerbe, O. (1994). Determination of the backbone torsion angle ε in nucleic acids. *J. Biomol. NMR* **4**, 595–601.
34. Gorenstein, D.G. (1981). Nucleotide conformational analysis by ^{31}P nuclear magnetic resonance spectroscopy. *Annu. Rev. Biophys. Bioeng.* **10**, 355–386.

35. Quigley, G.J. & Rich, A. (1976). Structural domains of transfer RNA molecules. The ribose 2′ hydroxyl which distinguishes RNA from DNA plays a key role in stabilizing tRNA structure. *Science* **194**, 796–806.
36. Szewczak, A.A. & Moore, P.B. (1995). The sarcin/ricin loop, a modular RNA. *J. Mol. Biol.* **247**, 81–98.
37. Fountain, M.A., Serra, M.J., Krugh, T.R. & Turner, D.H. (1996). Structural features of a six-nucleotide RNA hairpin loop found in ribosomal RNA. *Biochemistry* **35**, 6539–6548.
38. SantaLucia, J. & Turner, D.H. (1993). Structure of $(rGGCGAGCC)_2$ in solution from NMR and restrained molecular dynamics. *Biochemistry* **32**, 12612–12623.
39. Huang, S., Wang, Y.-X. & Draper, D.E. (1996). Structure of a hexanucleotide RNA hairpin loop conserved in ribosomal RNAs. *J. Mol. Biol.* **258**, 308–321.
40. Schweisguth, D.C. & Moore, P.B. (1997). On the conformation of the anticodon loops of initiator and elongator methionine tRNAs. *J. Mol. Biol.* **267**, 505–519.
41. Murphy, F.L. & Cech, T.R. (1994). GAAA tetraloop and conserved bulge stabilize tertiary structure of group I intron domain. *J. Mol. Biol.* **236**, 49–63.
42. Pley, H.W., Flaherty, K.M. & McKay, D.B. (1994). Model for an RNA tertiary interaction from the structure of an intermolecular complex between a GAAA tetraloop and an RNA helix. *Nature* **372**, 111–113.
43. Cate, J.H., *et al*., & Doudna, J.A. (1996). Crystal structure of a group I ribozyme domain: principles of RNA packing. *Science* **273**, 1677–1685.
44. Heus, H.A. & Pardi, A. (1991). Structural features that give rise to the unusual stability of RNA hairpins containing GNRA loops. *Science* **253**, 191–194.
45. Jucker, F.M. & Pardi, A. (1995). GNRA tetraloops make a U-turn. *RNA* **1**, 219–222.
46. Czworkowski, J., Wang, J., Steitz, T.A. & Moore, P.B. (1994). The crystal structure of elongation factor G complexed with GDP at 2.7 Å resolution. *EMBO J.* **13**, 3661–3668.
47. Nissen, P., Kjeldgaard, M., Polekhina, G., Reshetnikova, L., Clark, B.F.C. & Nyborg, J. (1995). Crystal structure of the ternary complex of phe-tRNA-phe, EF-Tu, and a GTP analog. *Science* **270**, 1464–1472.
48. Moore, P.B. (1995). Ribosomes seen through a glass less darkly. *Structure* **3**, 851–852.
49. Allain, F.H.-T., Gubser, C.C., Howe, P.W.A., Nagai, K., Neuhaus, D. & Varani, G. (1996). Specificity of ribonucleoprotein interaction determined by RNA folding during complex formation. *Nature* **380**, 646–650.
50. Gubser, C.C. & Varani, G. (1996). Structure of the polyadenylation regulatory element of the human U1A pre-mRNA 3′-untranslated region and the interaction with the U1A protein. *Biochemistry* **35**, 2253–2267.
51. Oubridge, C., Ito, N., Evans, P.R., Teo, C.-H. & Nagai, K. (1994). Crystal structure at 1.92 Å resolution of the RNA binding domain of the U1A spliceosomal protein complexed with an RNA hairpin. *Nature* **372**, 432–438.
52. Greenbaum, N.L., Radhakrishnan, I., Patel, D. & Hirsh, D. (1996). Solution structure of the donor site of a *trans*-splicing RNA. *Structure* **4**, 725–733.
53. Milligan, J.F. & Uhlenbeck, O.C. (1989). *Methods Enzymol.* **180**, 51–62.
54. Batey, R.T., Battiste, J.L. & Williamson, J.R. (1995). Preparation of isotopically enriched RNAs for heteronuclear NMR. *Methods Enzymol.* **261**, 300–322.
55. Simon, E.S., Bednarski, M.D. & Whitesides, G.M. (1988). Generation of cytidine 5′-triphosphate using adenylate kinase. *Tetrahedron Letters* **29**, 1123–1126.
56. Simon, E.S., Grabowski, S. & Whitesides, G.M. (1990). Convenient synthesis of cytidine 5′-triphosphate, guanosine 5′-triphosphate, and uridine 5′-triphosphate and their use in the preparation of UDP-glucose, UDP-glucuronic acid, and GDP-mannose. *J. Org. Chem.* **55**, 1834–1841.
57. Saenger, W. (1984). *Principles of Nucleic Acid Structure*. Springer-Verlag, New York.
58. Brünger, A.T. (1992). *X-PLOR Version 3.1: A System for Crystallography and NMR*. Yale University, New Haven, CT.